CHARACTERISTICS OF A FREELY ROTATING PARTICLE SEPARATOR FOR POLYDISPERSE MATERIAL

V. L. Zhokhov, A. L. Genkin, and A. A. Krivenko

UDC 621.359.484

A model has been developed and systematic calculations have been performed for particle motion in a self-rotating separator, with the results compared with experiments on a special tester.

Rotating blade sets are used to isolate particles of polydisperse material from gas flows. The particles are uniformly distributed in the flow at the inlet and are acted on by centrifugal forces in the channels between the blades and are thus displaced towards the edges of the blades, where they are received into dust chambers. Fast motors are usually employed to drive such separators. One can use a separator that employs a gas bearing and has blades with double-convex curvatures to avoid the use of a motor, since the blade sets represent a kinematically and aerodynamically coupled turbocompressor of almost zero power. The gas pressure is increased in the leading part of the channel between the compressor blades, and then the excess pressure is released in the exit (turbine) part of the channel. That design reduces the total pressure drop across the self-rotating separator considerably [1]. The blades are hollow and have porous surfaces in the compressor part and with open peripheral sections. The dust particles primarily interact with the concave surface in the compressor part, which governs the point where the porous surface (grid) is installed, through which the dust passes from the channel between blades to the internal blade cavity. The air passes through the narrow gap in the gas bearing into the blade and moves along the porous surface towards the open peripheral section, thus entraining the particles and transferring them to the collector [2]. Figure 1 shows the separator in dismounted form.

The speed of the blade assembly is comparatively low (ω = 20-60 Hz) and the separation performance is substantially dependent on the particle size, the aerodynamic parameters, and particularly the interaction of the particles with the blade surfaces. There are considerable difficulties in incorporating all the various factors governing the concentration because it is necessary to integrate the equations describing the two-phase turbulent flow.

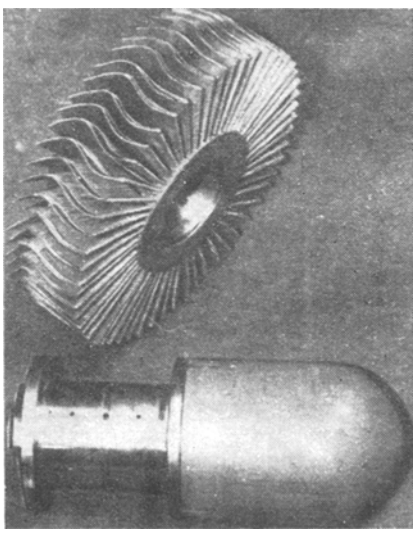

Fig. 1. Rotor with gas bearing housing and mount with sleeve in self-driven separator.

Translated from Inzhenerno-fizicheskii Zhurnal, Vol. 61, No. 2, pp. 262-267, August, 1991. Original article submitted May 5, 1990.

0022-0841/91/6102-1007$12.50

For relatively low bulk concentrations ($\beta \leq 10^{-4}$), one can neglect the particle–particle interactions and the effects on the flow [3], when one can derive the dust distribution and thus the separation performance on calculations for a polydisperse material with a given gas speed.

There are several papers on dust motion in blade channels in turbines, which usually deal with the initial stage of motion before the particles interact with the solid surfaces, while the gas flow is taken as two-dimensional [4, 5]. In [6], the three-dimensional gas flow in a rotating assembly was incorporated approximately by interpolation between the two-dimensional results for various radii in the assembly.

We have calculated the paths in a three-dimensional flow in the blade channels on the basis of the interaction with the surfaces in order to examine the separation performance in a self-rotating blade assembly.

We consider fairly small particles (10 μm ≤ δ ≤ 200 μm) for characteristic gas speeds (10 ≤ C ≤ 100 m/sec). We assumed $\rho_p/\rho \gg 1$, $(\rho D/\rho_p \delta) \sim 1$, $\mathrm{Re} = CD/\nu \gg 1$, and neglected the Archimedean force and the forces related to the pressure and velocity gradients, the acceleration of the adjoint mass, and the Basset force [7]. The equation of motion then retains only the aerodynamic resistance, the gravitational force, and the Magnus force. That equation is as follows in projections on the axes of the cylindrical (r, φ, z) coordinate system in the rotating separator array:

$$\frac{dc_r}{dt} = \frac{(\omega r + c_\varphi)^2}{r} + \frac{3}{4}\xi\frac{\rho}{\delta\rho_p}|C_r - c_r|(C_r - c_r) + 2\frac{\rho}{\rho_p}[(C_\varphi - c_\varphi)\Omega_z - (C_z - c_z)\Omega_\varphi]$$

$$\frac{dc_z}{dt} = \frac{3}{4}\xi\frac{\rho}{\delta\rho_p}|C_z - c_z|(C_z - c_z) + 2\frac{\rho}{\rho_p}[(C_r - c_r)\Omega_\varphi - (C_\varphi - c_\varphi)\Omega_r], \qquad (1)$$

$$\frac{dc_\varphi}{dt} = 2\omega c_r - \frac{c_\varphi c_r}{r} + \frac{3}{4}\xi\frac{\rho}{\delta\rho_p}|C_\varphi - c_\varphi|(C_\varphi - c_\varphi) + 2\frac{\rho}{\rho_p}[(C_z - c_z)\Omega_r - (C_r - c_r)\Omega_z].$$

System (1) is in dimensionless form, with the scale factors taken as the inlet gas speed C_0, the sleeve radius r_s of the blade assembly, and the ratio of these for the time and angular velocity. With the values used for the parameters, the Reynolds nubmer is $\mathrm{Re}_\delta = (C - c)\delta/\nu$ and ranges over $1 \leq \mathrm{Re}_\delta \leq 500$, while the resistance coefficient $\xi(\mathrm{Re}_\delta)$ is [3]:

$$\xi = (24/\mathrm{Re}_\delta + 4\sqrt[3]{\mathrm{Re}_\delta})K. \qquad (2)$$

We used the [3] dependence for K, which includes the effect from particle asphericity, and which is related to the geometrical shape factor f and Re_δ. It was assumed that the particles at the inlet to a channel were not rotating (Ω = 0) and that rotation arose only from interaction with the blade surfaces. The components of the angular and relative velocity vectors after collision are given by planar impact theory [8]:

$$\begin{aligned} c_{z2} &= K_1(C_{z1}\cos 2\alpha_b - c_{\varphi 1}\sin 2\alpha_b), \quad \Omega_{z2} = \pm c_{r1}/\delta; \\ c_{\varphi 2} &= -K_1(c_{z1}\sin 2\alpha_b - c_{\varphi 1}\cos 2\alpha_b), \quad \Omega_{\varphi 2} = 0; \\ c_{r2} &= K_1 c_{r1}, \quad \Omega_{r2} = \mp c_{z1}\cos\alpha_b/\delta \pm c_{\varphi 1}\sin\alpha_b/\delta, \end{aligned} \qquad (3)$$

in which the ± signs relate correspondingly to the concave and convex surfaces in the compressor part, while the energy accommodation coefficient K_1 was taken as constant at 0.8; α_b is the angle between the tangent to the boundary surface in a channel and the plane of reference, whose values are governed by the profile geometry. The reference plane φ = 0 was taken as the plane passing through the radial inlet and outlet edges in the compressor part of a blade. Vector Ω after ricochet in the flow is reduced because of friction with the gas. For $\mathrm{Re}_{\omega,\delta} \geq 10$, the damping rate for the angular velocity is [9]

$$\Omega(\bar{t}) = \Omega_2[1 + 4{,}76\rho\,\mathrm{Re}_{\omega,\delta}^{-1/2}\rho_p^{-1}\bar{t}]^{-2}, \qquad (4)$$

in which $\Omega(\bar{t})$ is the angular velocity at $\bar{t} = \Omega t$.

We derive the three-dmensional gas-velocity pattern in the channels by the [10] method. As $C_r = f(r, z)$ is calculated near the blade edges with appreciable error, it was refined by operating the separator in a wind tunnel, in which $C_r(z)$ was measured in the gap between the body of the separator and the blades for various gas flow rates through the receiving chambers.

System (1)-(4) was integrated by the Runge–Kutta method with the boundary conditions

$$C_{z0} = 1,\ C_{r0} = C_{\varphi 0} = 0,\ c_{z0} = 1 - c_s\ ,\ c_{\varphi 0} = \omega r,$$
$$c_{r0} = 0 \quad \text{at} \quad t = 0\,(z = 0), \tag{5}$$

in which the particle suspension velocity c_s is given by

$$c_s^2 = \frac{4}{3}\,\frac{\rho_p - \rho}{\rho}\,g\,\frac{\delta}{\xi}\ . \tag{6}$$

The gas speed C was specified at the nodes of a three-dimensional cylindrical coordinate system from preliminary calculations, while the coordinates for the boundary surfaces were defined at the points of intersection between the coordinate lines in the grid and the profile surfaces. Linear interpolation was used for values at intermediate points. The double-convex blades have radial profiles even for small solid-angle thicknesses only for two values of the z coordinates: z = 0 and z = z_1, where z_1 is the coordinate of the exit edge in the compressor part, so one describes how the coordinates $\varphi_{b,\pm}$ of the boundary surfaces vary with radius by means of $\varphi_{b,\pm} = a_{n,\pm} r + b_{n,\pm}$, in which the coefficients $a_{n,\pm}$ and $b_{n,\pm}$ were taken as constant for $z_n \le z < z_{n+1}$ (n is the number of the corresponding node along the z coordinate). The paths were calculated with the volume in one blade channel split up into 108 parts (n = 6 along the z axis, k = 3 along the φ axis, and i = 6 along the r axis), i.e., the inlet section at z = 0 was divided into 18 cells. It was assumed that the particles with their various sizes entered the channel from the centers of the cells in amounts proportional to their mass distributions. Figure 2a shows several paths for δ = 11.9, 68.3, and 118.5 μm in the (z, φ) plane for the average radius of the separator. The finely divided components, no matter what the point of entry to the channel, interact repeatedly with the blade surfaces and move almost along the performations in the compressor parts. A large particle after one or two impacts ricochets, and because of its comparatively high inertia, interacts with the opposite boundary surface. The number of collisions for a particle having δ = 11.9 μm with the perforations is 3-12, as against 1-3 for δ = 118.5 μm. A basic mode parameter is the speed ω, which increases with the setting angle γ in the turbine part of the profile for a fixed inlet speed. Figure 3 shows paths for particles having δ = 11.9 μm entering the channel near the root section of the blade for various ω. For $\omega > 2.2 \cdot 10^3$ sec^{-1}, the particles are ejected into the collector essentially after one collision. For $10^3 < \omega < 2 \cdot 10^3$ sec^{-1}, after collision with the profile, a particle may move towards the inlet section (curves 6 and 7). These results have been obtained without allowance for turbulent fluctuations in C, i.e., we used averaged values $\langle C_z \rangle$, $\langle C_r \rangle$, $\langle C_\varphi \rangle$. For high Re, the turbulence intensity attains $\varepsilon = \dfrac{\sqrt{\langle C'^2 \rangle}}{\langle C \rangle}$ = 0.1-0.2, and the fluctuations in the velocity components are almost normally distributed with relative standard deviation ε and mathematical expectation $\langle C_z \rangle$, $\langle C_r \rangle$, $\langle C\varphi \rangle$. The velocity components were simulated in accordance with the following in order to correct for the effects of the pulsations on the paths:

$$C_m = \langle C_m \rangle + \varepsilon \left(\sum_{i=1}^{12} p_i - 6 \right),\ m = r,\ \varphi,\ z, \tag{7}$$

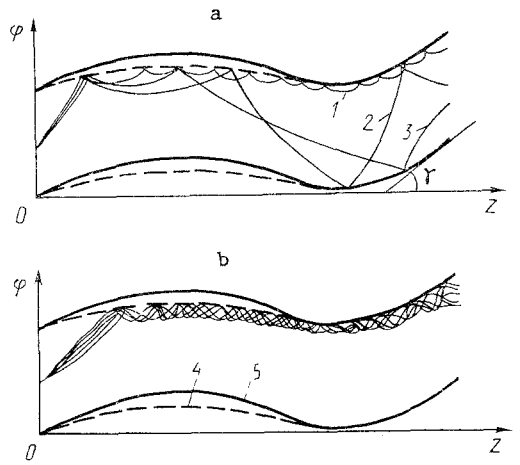

Fig. 2. Paths in separator: a) uncorrected for turbulent gas pulsations (1 – δ = 11.9 μm; 2) 68.3; 3) 118.5); b) corrected for pulsations, δ = 11.9 μm; 4) grid; 5) blade body.

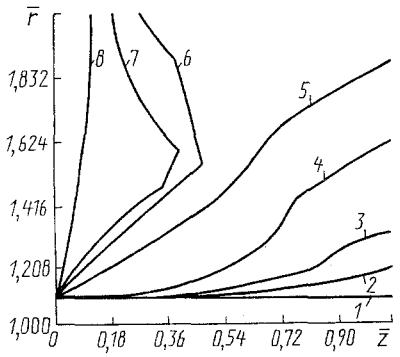

Fig. 3. Particle paths (δ = 11.9 μm) for separator angular velocities of: 1) ω = 0; 2) 10 sec^{-1}; 3) 38 sec^{-1}; 4) 300; 5) 400; 6) 10^3; 7) $2.3 \cdot 10^3$; 8) 10^4.

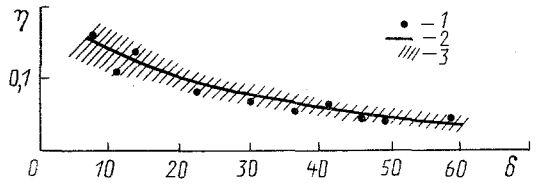

Fig. 4. Separator performance as a function of median particle diameter (ω = 38 sec^{-1}, C = 25 m/sec, μ_0 = 140 mg/m^3): 1) experimental results; 2) calculation unconnected for turbulent pulsations; 3) wind convection; δ in μm.

in which p_i are random numbers in the range $0 \leq p \leq 1$ with uniform distributions. Figure 2b shows paths for δ = 11.9 μm particles entering a channel at the average radius with allowance for the fluctuations. The width of the spread may attain 30% of the grating pitch, while the numbers of impacts on the blades increase appreciably.

The perforated concave surface in the compressor part is usually provided by a metal grid. It was assumed that the equivalent cell diameter was d_e = 0.6 mm and wire thickness 0.3 mm. With such a grid, about 52% of the particles ricochet in each interaction with the wires, while the others pass into the blades and are ejected via the open periphery. Path calculations enabled us to determine the optimum position for the receiving chamber. To provide high performance $\eta = m_k/m_0$, in which m_0 and m_k are the total masses of the particles in the inlet and exit tubes, the chamber should be placed downstream from the blade assembly by $l \approx 0.3b$, in which b is the blade chord, while the diameter of the exit tube should be 15-20% less than the separator diameter. Figure 4 shows the dependence of η on the median diameter for a polydisperse material for one mode of operation. The hatched region corresponds to the spread in separation capacity when one corrects for the turbulent pulsations. We also show measurements made on testing the separator. A detailed description has been given of the tester and the methods and results in [2]. There is good agreement between theory and experiment, which shows that the method adequately describes the motion in such a separator, which provides a high degree of purification from dust ($\eta \approx 0.05$).

NOTATION

ω, separator rotational frequency; β, bulk particle concentration; δ and f, particle diameter and geometrical shape factor; ρ, density; D, separator diameter; C_r, C_φ, C_t, c_r, c_φ, c_z, projections of the gas and particle velocity vectors on the (r, φ, z) coordinate-system axes; ξ and ν, aerodynamic resistance coefficient and kinematic viscosity; Ω_r, Ω_φ, Ω_z, projections of the particle-rotation angular velocity on the coordinate axes; α, angle between tangent to boundary surface in channel and (φr, z) reference plane; a and b coefficients defining the dependence of the φ coordinates of the boundary surfaces on radius ($\varphi = a + br$); ε, turbulent pulsation intensity; $\langle C \rangle$, averaged values of gas velocity vector projections; η, separation performance; m, total particle mass; Re, Reynolds number. Subscripts: p, particle; 0, at inlet to separator; 1 and 2, values before and after impact correspondingly; ±, quantities relating to convex and concave surfaces of blades respectively.

LITERATURE CITED

1. V. L. Zhokhov, Énergomashinostroenie, No. 8, 6-8 (1986).

2. V. L. Zhokhov and A. A. Krivenko, Dvigatelestroenie, No. 6, 43-45 (1989).
3. Z. R. Gorbis, Heat Transfer and Hydromechanics for Particle-Bearing Flows [in Russian], Moscow (1970).
4. M. E. Deich, V. I. Kiryukhin, G. A. Filippov, and O. A. Povarov, Teplotekhnika, No. 8, 20-23 (1974).
5. Bigger, Tabakoff, and Hamed, Proc. ASME, Power Machines Plant, 104, No. 1, 43-51 (1982).
6. M. F. Husslin and W. Tabakoff, J. Aircraft, 10, No. 7, 434-440 (1973).
7. S. L. Sow, Multiplase-System Hydrodynamics [Russian translation], Moscow (1971).
8. W. Goldschmidt, Collisions: Theory and Physical Properties of Colliding Bodies [Russian translation], Moscow (1965).
9. Yu. N. Krivenko, Hydromechanics [in Russian], Issue 16, Kiev (1970), pp. 57-62.
10. M. I. Zhukovskii, Aerodynamic Calculations on Axial Turbines [in Russian], Leningrad (1967).

EXTRUSION RHEODYNAMICS FOR A VISCOUS COMPRESSIBLE MATERIAL

L. S. Stel'makh, A. M. Stolin, and B. M. Khusid

UDC 532.135

An analytic solution is derived for the consolidation and flow of a viscous compressible material used in plunger extrusion, which enables one to determine the density, velocity, and stress patterns in the specimen and in the rod.

Components are increasingly prepared from refractory powders by plunger extrusion, in which the material is extruded from a press mold through a die.

Good models exist for such extrusion for incompressible plastic and viscous materials [1-5] such as most polymer and metal systems. However, those models are sometimes inapplicable for refractory compressible powder composites. Such a material behaves as a viscous or viscoplastic body only over 1000°C, so external heating is used (hot extrusion [7, 8]). The latter method can give components from powders that do not press well. The rheological behavior and the combination of deformation and consolidation mean that such systems must be considered separately. The features are reflected in consolidation theory for a viscous compressible material, which can be based on a rheological approach [9, 10]. Numerous papers deal with axial compression for a viscous porous material [11-14]. Here we consider the extrusion of a viscous compressible material from a chamber via a slot. The model and the method are used with Lagrangian coordinates to obtain an analytic solution for the density and velocity distributions in the chamber and in the rod.

Model and Main Assumptions. We consider the flow of a viscous porous material from a cylindrical chamber bounded above by a moving piston. The initial length of the material is H_0, and the radius of the cross section is r_0. At the bottom of the chamber there is a circular hole with radius r_1 through which the material is extruded into a cylindrical guide of the same radius. The symmetry axis is taken as the z axis, whose positive direction is opposite to that of the piston motion. The origin $z = 0$ lies at the center of the exit cross section from the chamber. We neglect the friction on the walls of the chamber and guide cylinder and affects from bulk forces.

The flow region is divided into two parts: within the chamber between the piston at $z = H(t)$ and the exit section $z = 0_+$ and that within the guide between $z = 0_-$ and the free surface $z = L(t)$. The subscripts + and − indicate correspondingly that the $z = 0$ section relates either to the chamber or to the guide. We neglect perturbations in the two parts of the flow on passage from the chamber to the hole. The motion in each region is taken as steady-state and one-dimensional with one nonzero velocity component $v_z = v \neq 0$. If the

Structural Macrokinetics Institute, Academy of Sciences of the USSR, Chernogolovka.
Translated from Inzhenerno-fizicheskii Zhurnal, Vol. 61, No. 2, pp. 268-276, August, 1991. Original article submitted August 6, 1990.

0022-0841/91/6102-1011$12.50